

Growth of Diffusion Limited Aggregation (DLA)-Like Branched Patterns in a Belousov–Zhabotinskii Type Reaction System

Narendra Yadav*[1,2] and Prem Kumar Srivastava[1]

[1]Department of Applied Chemistry, Birla Institute of Technology, Mesra-835 215, Ranchi, India

[2]Department of Space Engineering and Rocketry, Birla Institute of Technology, Mesra-835 215, Ranchi, India

Received September 7, 2010; E-mail: yadav_chemistry@rediffmail.com

The Belousov–Zhabotinskii (BZ) type reaction system with dual organic substrate, which leads to growth of tree/bush-like crystal patterns has been studied. The reaction system has been found to exhibit concentric ring patterns, starting with propagation of waves in the solution state. A colloidal state, composed of numerous fine solid particles, has been observed during the reaction. These particles have been found to initially form dendritic nucleation centers and subsequently grow into tree/bush-like crystal patterns by self-aggregation. A possible reaction mechanism has been proposed. Based on a diffusion limited aggregation (DLA) mechanism, fractal characteristics and aggregation behavior of tree/bush-like patterns are also discussed.

Some chemical systems far from equilibrium occasionally show regular changes of concentrations of intermediates in space or time under specific reaction conditions. A well-known example is the Belousov–Zhabotinskii (BZ) reaction systems,[1–6] which involve oxidation of organic substrates by bromate ions in acidic medium. The reaction is catalyzed by trace transition-metal ions (in free states or in complexes) often in two oxidation states which differ by a single electron. When the reaction solution is adequately stirred, the color changes periodically as a function of time. The phenomenon has been characterized as chemical oscillations with a period usually of the order of tenths of seconds to a few minutes, depending upon the concentration of the reagents and catalyst. On the other hand, when the same reaction is performed in a thinner layer (thickness $\approx$1 to 2 mm) of the solution placed in a Petri dish, fascinating spatiotemporal patterns such as concentric rings, spiral bands, and traveling waves are observed.

Similarly, many spatial or rhythmic crystal patterns during crystallization of Liesegang systems, crystalline polymers, and organic and inorganic materials have also been reported.[7–10] The study of these crystallization behaviors and stability of such structures has generated considerable interest in structure–property relationships of various functional materials.[11] It is generally believed that the morphology of these crystal patterns is strongly dependent on the reaction conditions and the distance from the thermodynamic equilibrium state. As the distance from equilibrium is increased, the growth patterns are found to transition from stable crystal faces to ramified structures, associated with changes in surface energy. Moreover, morphology of crystal patterns may also be altered by many other determining factors, such as driving force, concentration gradients, and diffusion fields.[12,13]

Considerable effort has been made to understand the growth process, especially the effect of macroscopic driving force and interfacial dynamics. Physical analysis based on interfacial dynamics has also been carried out to understand the formation of various complex and densely branched patterns.[14] It is well established that anisotropy and fluctuations (concentration, temperature, diffusion, ion convection, etc.) are the two controlling factors which influence the complex interfacial structure, as well as the stability of the morphology of crystal patterns. Anisotropy may limit the growth of crystals in certain directions to form ordered crystal patterns, whereas fluctuations often give rise to fractal-like morphology.[15–17]

Diffusion limited aggregation (DLA) methods have been used to describe the growth behavior and fractal complexity during pattern formation. This method involves a very simple algorithm which can produce highly intricate structures by random aggregation of particles. DLA-like patterns have also been observed in various crystallization phenomena usually at far equilibrium conditions, such as electrodeposition, bacterial colonies, colloidal aggregates, dendrite formation, viscous fingering, and many others.[16–20] Thus, the DLA methods have been widely used to explain and analyze the fractal aggregation phenomenon.

A variety of spatiotemporal patterns have been observed during solution-phase reaction, which has been explained by the reaction–diffusion (RD) mechanism of BZ reaction systems. The growth of tree/bush-like crystal patterns comes under a new investigation toward crystal growth associated with DLA mechanism and the BZ reaction processes. This experiment has been carried out with dual organic substrates which exhibit wave propagation and concentric ring patterns in solution-phase reaction. Besides this, a colloidal phase, consisting of numerous fine particles has been observed during reaction. These particles have been found to initially form dendritic nuclei centers and subsequently to grow into tree/bush-like crystal patterns which may be attributed to self-aggregation. An attempt has been made to propose possible reaction equations for solution-phase reaction and associated reaction mechanism for the growth of tree/bush-like crystal patterns. Transition in morphology of crystal patterns has been

Published on the web May 7, 2011; doi:10.1246/bcsj.20100258

found in the range of organic substrate, which has been described and discussed.

Experimental

Succinic acid (SA), ethyl acetoacetate (EAA), and iron(II) sulfate (CDH India Ltd.), 1,10-phenanthroline, and ammonium cerium(IV) sulfate (Ce^{4+}) (E-Merck), potassium bromate ($KBrO_3$), and sulfuric acid (H_2SO_4) (S.D. fine chemicals, India Ltd.) of AR grade were used for the experimentation. All the experiments were performed in a flat Petri dish of 9.1 cm (i.d.). Stock solutions of SA (5% w/v), $[EAA] = 0.8\,mol\,dm^{-3}$, and ferroin $[[Fe(phen)_3]^{2+}] = 0.025\,mol\,dm^{-3}$ were prepared in doubly distilled water (DDW). The ferroin indicator used was prepared by homogenous mixing of 1,10-phenanthroline and iron(II) sulfate in a molar ratio of 3:1 in DDW. Stock solution of the $KBrO_3$ and Ce^{4+} (5% w/v) was prepared in $[H_2SO_4] = 1.5\,mol\,dm^{-3}$.

2 mL of SA, EAA, Ce^{4+}, and H_2SO_4, along with 1.0 mL of $[Fe(phen)_3]^{2+}$ was mixed in a 100 mL beaker and made homogenous by constant shaking. Then 2 mL of the $KBrO_3$ solution was added to the resultant mixture and was well shaken to maintain homogeneity. This stage was marked as initiation of the reaction. Thereafter, half of the reaction mixture (6.5 mL) was immediately taken out from the bulk solution and spread in a Petri dish with uniform thickness ($\approx$1 mm). The resultant concentrations of reactants were calculated as $[EAA] = 0.1212\,mol\,dm^{-3}$, $[SA] = 0.1016\,mol\,dm^{-3}$, $[Ce^{4+}] = 0.00486\,mol\,dm^{-3}$, $[KBrO_3] = 0.0553\,mol\,dm^{-3}$, $[[Fe(phen)_3]^{2+}] = 0.0038\,mol\,dm^{-3}$, and $[H_2SO_4] = 0.42\,mol\,dm^{-3}$.

The study of morphology and structure of the crystal patterns was carried out by optical microscope (OPM) (Leica, EZ4D) at a specific magnification and scanning electron microscope (SEM) (Jeol, JSM 6390LV) coupled with energy-dispersive spectrum (EDS) technique under vacuum, at an accelerating voltage of 20 kV. Gas chromatography mass spectrometry (GC-MS) (Perkin-Elmer GC-MS Clarus 500) associated with Elite Column with a length of 20 cm and internal diameter of 0.18 μm, was used to identify the possible compositions of tree/bush crystal patterns. The particle size analysis was carried out by Dynamic light scattering (DLS) (Malvern, Zeta-Sizer NANO ZS). The crystal materials were characterized with an X-ray powder diffractometer (Rigaku, Model, Miniflex-2005B111) equipped with Cu Kα ($\lambda = 1.54$ Å) operating at a tube load 100 V:10 A and 50/60 Hz. Each sample was scanned in a (2θ) range between 10 to 80° with a scan rate of 0.2°/3 s. The infrared spectra (Shimadzu, IR Prestige- 21 FTIR instrument) of the tree/bush crystal samples were recorded at a resolution of $4\,cm^{-1}$ and 64 scans.

Results

It has been observed that the system shows a complex behavior during reaction. The reaction system also exhibits multisequential reaction steps, and each step has been found to produce distinct pattern quality, however it has some diverse characteristics for subsequent reaction. In order to simplify the complexity of the pattern formation, the study has been carried out under four distinguishable headings, namely (a) solution-phase reaction, (b) colloidal state and solid-phase nucleation, (c) growth of tree/bush-like crystal patterns, and (d) morphological transition of crystal patterns.

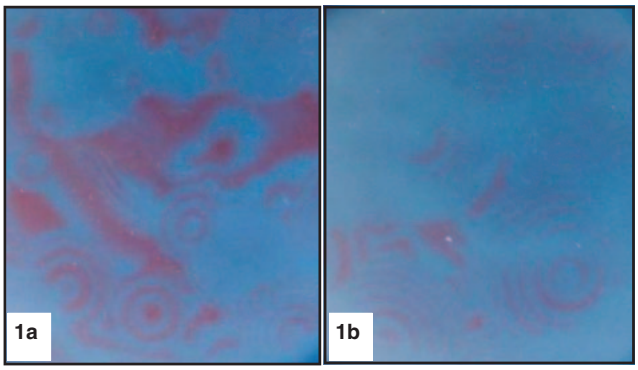

Figure 1. Development of concentric rings at solution-phase reaction, after (1a) 12 and (1b) 20 min from the beginning of the reaction. The initial concentration corresponds to $[EAA] = 0.1212\,mol\,dm^{-3}$, $[SA] = 0.1125\,mol\,dm^{-3}$, $[Ce^{4+}] = 0.00486\,mol\,dm^{-3}$, $[BrO_3^-] = 0.0553\,mol\,dm^{-3}$, $[H_2SO_4] = 0.420\,mol\,dm^{-3}$, $[[Fe(phen)_3]^{2+}] = 0.0038\,mol\,dm^{-3}$, Petri dish (i.d.) = 9.1 cm.

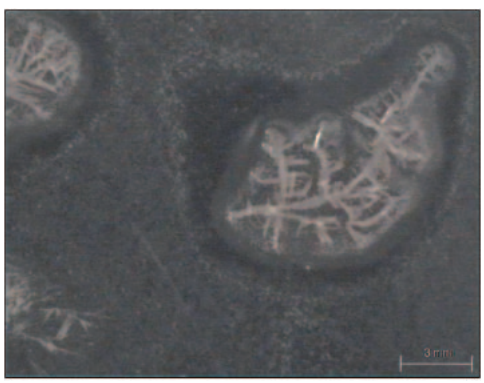

Figure 2. OPM microphotograph of dendritic nucleus structure.

In the solution-phase reaction, initially, fast appearing and disappearing red wave patterns were initially observed. Approximately 3 to 4 repeated cycles of red wave patterns were seen during the first 4 min. The frequencies of propagation of waves gradually decreased as reaction time elapsed. After 5 min, the stable red color nucleation was again observed, which propagated slowly on the blue background of the reaction solution. This resulted in the formation of concentric ring patterns, as shown in Figure 1. The process continued for the next 30 min. The specific reaction times were taken from the time of introduction of the BrO_3^- into the solution mixture.

After 15 h, the reaction showed a colloidal phase composed of numerous colloidal particles, which were embedded in the matrix of the reaction solution. These colloidal particles have been found to self-aggregate, and exhibit solid phase nucleation centers of dendritic character, as shown in Figure 2. The nuclei centers formed at early stage were found to dominate over the late stage nuclei centers, and exclusively took part in the growth process. A schematic representation of the proposed growth mechanism has been presented, as shown in Figure 3. Thereafter, in approximately 3 h, these nuclei centers grew

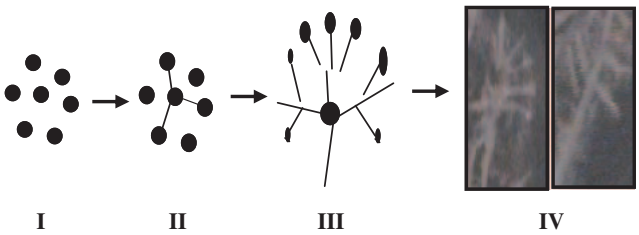

Figure 3. Schematic growth mechanism of dendritic nucleus structure.

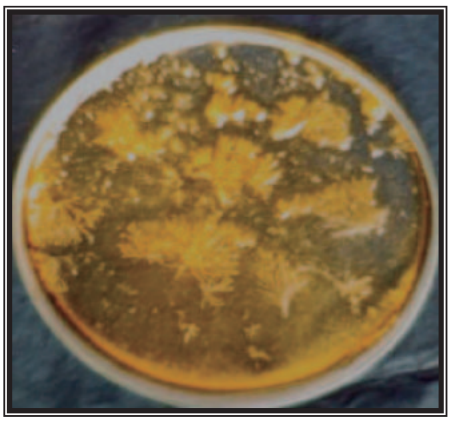

Figure 4. Morphology of tree/bush-like crystal patterns.

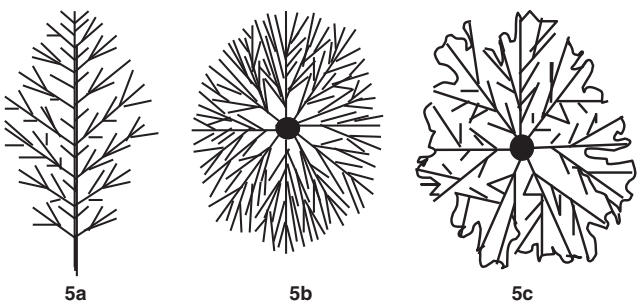

Figure 5. Graphical scheme of characteristic morphologies of (5a) tree/bush-like crystal patterns, (5b) spherulitic crystal patterns, and (5c) seaweed-like crystal patterns.

completely in size giving out tree/bush-like crystal patterns, as shown in Figure 4. The growth behavior of tree/bush-like patterns is illustrated in a graphical scheme (Figure 5a), and how their branching modes differ from a spherulite (Figure 5b) and also a seaweed-like crystal patterns (Figure 5c) are adequately discussed. The presence of metal ions and also the possible composition of the tree/bush structure have been confirmed by EDS spectra and GC-MS chromatogram, as shown in Figures 6 and 7 respectively. The transition in crystal morphology has been observed in the range of concentration of organic substrate, as shown in Figure 8.

The crystal units before the solid-phase nucleation have been characterized by SEM, as shown in Figure 9. It may be concluded from the results that tree/bush-like crystal patterns observed are formed by synchronized aggregation of the multi crystal phases. This observation is also supported by XRD and FTIR spectra, as shown in Figures 10 and 11 respectively.

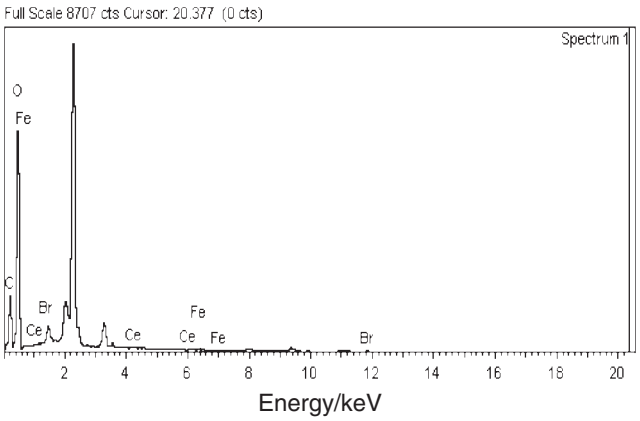

Figure 6. EDS spectrum of tree/bush-like crystal patterns.

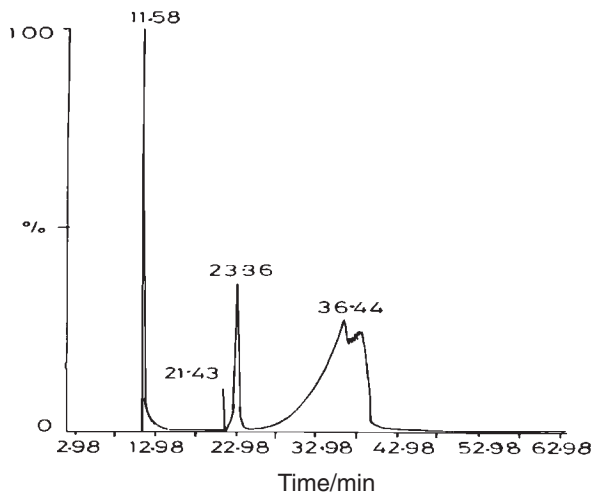

Figure 7. GC-MS spectrum of tree/bush-like crystal materials.

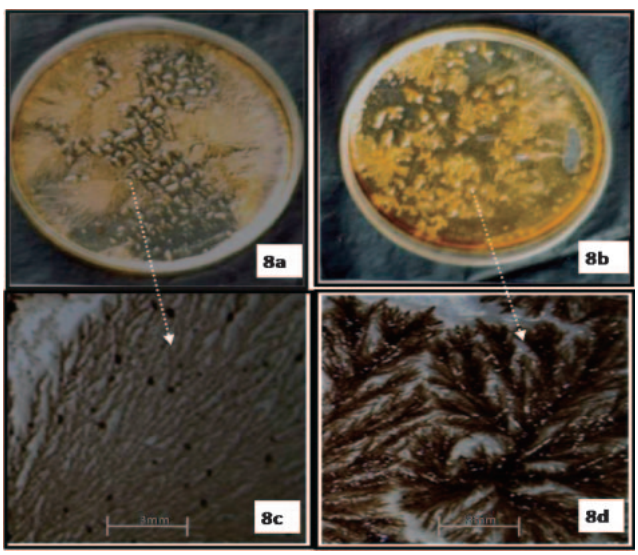

Figure 8. Transitions of crystal morphologies of (8a) densely branched or spherulitic morphology at [EAA] = 0.1225 mol dm^{-3} and (8b) seaweed-like crystal morphology at [SA] = 0.1380 mol dm^{-3}. The others reaction conditions are and same as described in Figure 1.

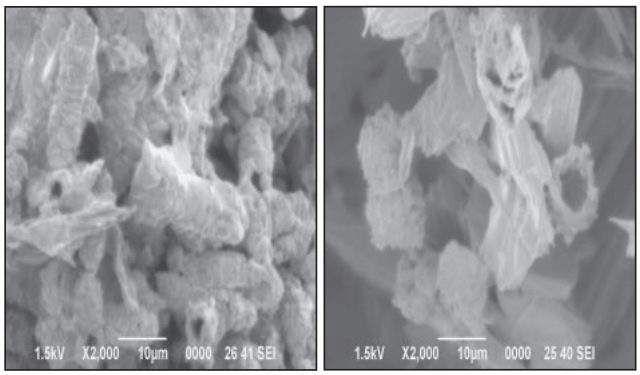

Figure 9. SEM microphotographs of crystal units during solid-phase nucleation (a), tubules-like structures may result by periodic stacking of disc-like crystal units as shown in (b).

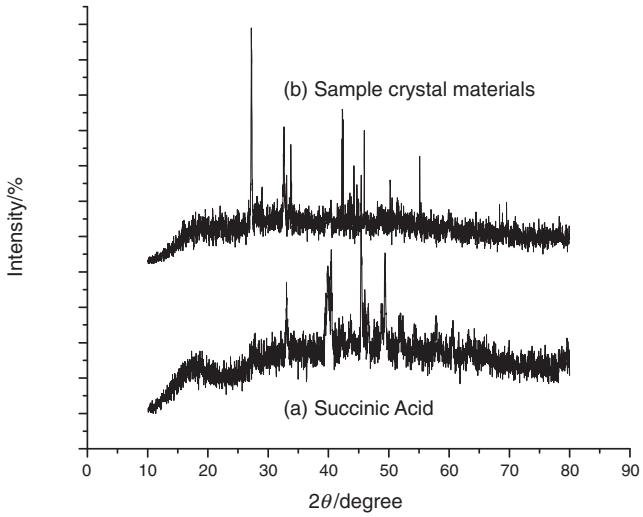

Figure 10. Powdered XRD spectra of (a) pure succinic acid and (b) tree/bush-like crystal materials.

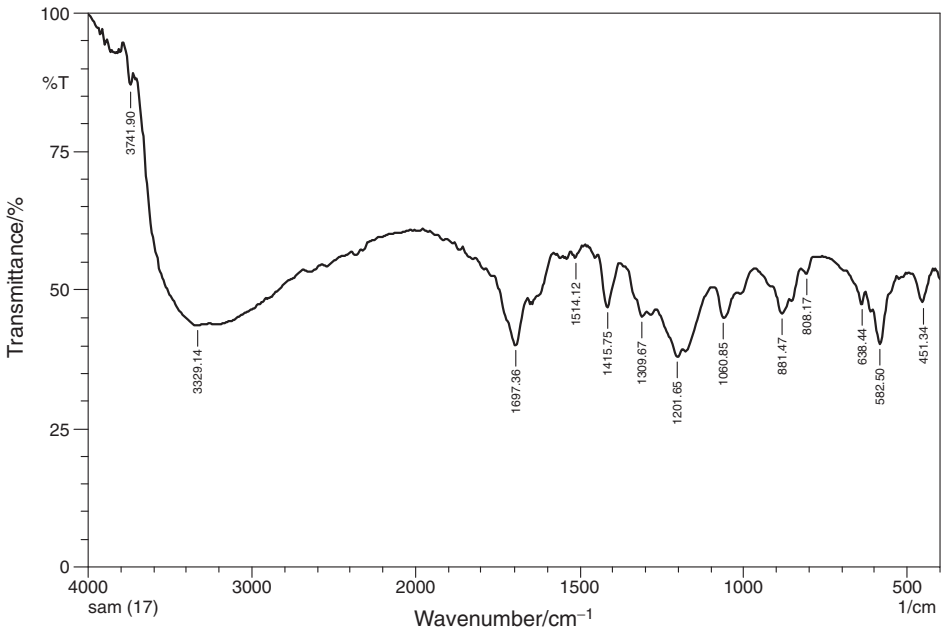

Figure 11. FTIR spectrum of tree/bush-like crystal materials.

Discussion

Solution-State Reaction. Ferroin, used as a redox indicator, intensifies the color changes during solution-phase reaction. Its color can vary between red and blue, which indicates the state of the reaction from reduced state to oxidized state respectively. The coloration mechanism may be helpful in analysis and the visual prediction of the spatiotemporal structures of waves and patterns, if the reaction is carried out in the unstirred form of thin solution layers. During the reaction, ferroin can change its form possibly between two physical states, as shown below:

$$\underset{\text{Ferroin}}{[\text{Fe(phen)}_3]^{2+}} \rightleftharpoons \underset{\text{Ferriin}}{[\text{Fe(phen)}_3]^{3+}} \quad (1)$$

(Reduced state) (Oxidized state)

Just after the initiation of the reaction, the red wave patterns have been found to appear and disappear in periodic manner. Subsequently, the reaction is found to bifurcate into some stable phase nucleation which slowly propagates and leads to formation of concentric ring patterns. It takes approximately 2 min for the second phenomenon to initiate. Hence, we can relate these two sequential phenomena to dual frequency of the oscillatory reaction.[21] While the high frequency is attributed to rapid emergence of the red wave patterns, the concentric ring patterns may be said to form in the range of the low frequency regime of the oscillatory reaction. The redox and RD mechanism significantly controls the pattern behavior under constraints of the reactions. Moreover, the reaction mechanism and pattern formation description are based on the fundamentals of BZ chemistry.[22–25] Under traces of Ce^{4+} (or Fe^{2+}), acting as catalyst and in acidic BrO_3^-, the EAA (or SA) is

oxidized. Some intermediates have also been formed whose concentrations have been found to vary periodically as a function of time. The RD mechanism may relocate newly formed product phases at regular intervals. By using this hypothesis, oscillatory behavior of solution-phase reaction could be elucidated. However the reaction is found to become complicated, when carried out under the solid-phase nucleation and crystal growth followed by colloidal-phase reaction. Instead, the qualitative aspects of pattern formation in the solution-phase reaction and their associated reaction mechanisms have been summarized in this section.

A number of investigations have been carried to describe the chemistry of the BZ reactions.[21–25] Based on these results, the overall reaction mechanism of the present study has been proposed as,

$$\mathrm{EAA} + \mathrm{BrO_3^-} + \mathrm{H^+} \rightarrow \underset{\mathbf{A}}{\text{Br-EAA}} + \underset{\mathbf{B}}{\text{HO-EAA}} + \mathrm{H_2O} + \mathbf{P} \quad (2)$$

where, product **A** is bromoethyl acetoacetate, **B** is hydroxyethyl acetoacetate, and **P** corresponds to some unidentified chemical entities. The reaction in eq 2 results from a series of reaction steps. The EAA does not react directly with BrO_3^-; instead, BrO_3^- is reduced to HOBr either by Br^- or by Ce^{3+} as shown in eqs 2a and 2b.

$$\mathrm{BrO_3^-} + 2\mathrm{Br^-} + 3\mathrm{H^+} \rightarrow 3\mathrm{HOBr} \quad (2a)$$

$$\mathrm{BrO_3^-} + 4\mathrm{Ce^{3+}} + 5\mathrm{H^+} \rightarrow \mathrm{HOBr} + 4\mathrm{Ce^{4+}} + 2\mathrm{H_2O} \quad (2b)$$

and then the HOBr formed in eq 2a or 2b reacts with EAA to form product **A**, as shown in eq 2c, the stoichiometry is maintained during the course of reaction as shown in eqs 2d and 2e,

$$\mathrm{HOBr} + \mathrm{EAA} \rightarrow \mathbf{A} + \mathrm{H_2O} \quad (2c)$$

$$\mathrm{HOBr} + \mathrm{EAA} \rightarrow \mathbf{B} + \mathrm{Br^-} + \mathrm{H^+} \quad (2d)$$

$$2\mathrm{Ce^{4+}} + \mathrm{EAA} + \mathrm{H_2O} \rightarrow 2\mathrm{Ce^{3+}} + \mathbf{B} + 2\mathrm{H^+} \quad (2e)$$

When EAA is oxidized, the concentration of product **A** may increase, resulting in slowing down of autocatalytic oxidation of Ce^{3+}. In such a condition, the reaction solution remains in reduced state. This reduces the rate of oxidation of EAA and the course of reaction now proceeds toward the formation of product **B**, whose concentration was supposed to increase with the progress of the reaction. Throughout the reaction, BrO_3^- is the key reagent which initiates the reaction and provides an oscillatory network of the reactions by forming a number of intermediates such as HOBr, $BrO_2^{\bullet}$, and Br^-. The concentration of these intermediates has effectively controlled the oscillatory behavior of the reaction by reacting together in feasible reaction routes. A possible reaction for intermediates has been summarized in equations from 2f to 2k,

$$\mathrm{BrO_3^-} + \mathrm{Br^-} + 2\mathrm{H^+} \rightarrow \mathrm{HBrO_2} + \mathrm{HOBr} \quad (2f)$$

$$\mathrm{HBrO_2} + \mathrm{Br^-} + \mathrm{H^+} \rightarrow 2\mathrm{HOBr} \quad (2g)$$

$$\mathrm{BrO_3^-} + \mathrm{HBrO_2} + \mathrm{H^+} \rightleftharpoons 2\mathrm{BrO_2^{\bullet}} + \mathrm{H_2O} \quad (2h)$$

$$\mathrm{BrO_2^{\bullet}} + \mathrm{Ce^{3+}} + \mathrm{H^+} \rightarrow \mathrm{HBrO_2} + \mathrm{Ce^{4+}} \quad (2i)$$

$$2\mathrm{HBrO_2} \rightarrow \mathrm{BrO_3^-} + \mathrm{HOBr} + \mathrm{H^+} \quad (2j)$$

$$\mathrm{Br^-} + \mathrm{HOBr} + \mathrm{H^+} \rightarrow \mathrm{Br_2} + \mathrm{H_2O} \quad (2k)$$

The intermediate reactions steps begin in the reduced state, as shown in eqs 2f and 2g, having high concentrations of Br^- ions. As the reaction progresses, Br^- ions are consumed during bromination and also for the oxidation of Ce^{3+} and EAA and produce enough $HBrO_2$, as shown in eqs 2h and 2i. When $HBrO_2$ diffuses to neighboring domains, it tends to produce concentration gradients between reduced and oxidized states. This has resulted in development of wave fronts which are composed of oxidizing phase waves and reducing phase waves, as observed during the reaction in the form of concentric ring patterns. Usually the reducing phase waves diffuse and propagate just after the oxidizing phase waves.[22–24] Interestingly, the reaction eq 2k shows the formation of Br_2 by reaction with intermediates, as proposed. It could lead the reaction solution into an oxidized state. Thus a cyclic reaction network has been accomplished between reduced state and oxidized state of the reaction system.

The periodical color changes were attributes to the rise and fall of the concentration of substrates (or derivatives) with regular intervals, which supports oscillatory behavior of the reaction. The coloration behavior of the reaction also suggested that ferroin must be involved in the process. Recently it has been demonstrated that ferroin alone could catalyze the BZ reaction as proposed for cerium.[1,22,25] The common intermediates (often $Br^-/HBrO_2$) coupled with $[Fe(phen)_3]^{3+}$ have been used to investigate the quantitative development of such kinds of phase waves. Based on this, possible reactions of the ferroin, acting as a catalyst are shown in following equations,

$$\mathrm{BrO_2^{\bullet}} + [\mathrm{Fe(phen)_3}]^{2+} + \mathrm{H^+} \rightarrow \mathrm{HBrO_2} + [\mathrm{Fe(phen)_3}]^{3+} \quad (3)$$

$$[\mathrm{Fe(phen_3)}]^{3+} + \mathbf{A}^{\bullet} + \mathrm{EAA} \rightarrow [\mathrm{Fe(phen)_3}]^{2+} + \mathrm{H^+} + \mathbf{A}^{\bullet} + \mathrm{EAA}^{\bullet} \quad (4)$$

$$\mathbf{A}^{\bullet} + \mathrm{EAA}^{\bullet} + \mathrm{H_2O} \rightarrow \mathrm{Br^-} + \mathrm{EAA} + \mathbf{P} \quad (5)$$

The reactions of eq 3 to eq 5 have also been monitored by Br^- and $HBrO_2$ which were produced in a similar reaction as described in earlier intermediate reaction steps. The two simultaneous reactions eqs 3 and 4 correspond to high concentration of $HBrO_2$ and low concentration of the bromo derivatives. In contrast to earlier reaction equations, the $HBrO_2$ could revive BrO_3^- for reinitiating the oscillatory reaction for extended periods similarly as proposed in the reaction eq 2h.

The overall solution-phase reaction exhibits waves and patterns under two oscillatory regimes. It is also evident that at least three color changes have occurred between two existing physical states of the ferroin. It reveals the high concentration of the Br^- and low concentration of $[Fe(phen)_3]^{3+}$ and $HBrO_2$ respectively in the reduced state. This condition can lead to decrease in the rate of formation of product **A** while rate of the formation of product **B** gradually increased. When the concentration of product **B** becomes sufficiently high it produces an inhibitory effect on oscillatory behavior of the reaction which can be why only two short lived oscillatory regimes are observed during the experiments.

Colloidal State and Solid-Phase Nucleation. The solid-phase nucleation phenomenon occurs after 15 h from the beginning of the reaction process. Initially, the system exhibits numerous fine solid particles embedded in the matrix of reaction solution, called the colloidal state. These particles play a major role in the solid-phase nucleation and subsequently in the growth of crystal patterns. The solid-phase nucleation that occur during the colloidal state of the reaction initially emerges in the form of certain discrete points called nucleus centers,

which are possibly formed by random aggregation of colloidal particles. It has also been observed that fine solid particles are distributed around the dendritic nucleation center. Thus a concentration gradient between nucleation centers and symmetrically distributed fine solid particles cannot be ignored. Under such conditions, a diffusion mediated aggregation process has been considered which can produce an organized nucleus structure. In early phase, this structure has large surface of curvature and might be composed of mesoscopic crystals which attributes high surface energy. Therefore, further growth can lead to the formation of stable and specified geometric crystal pattern which was essentially monitored by lowering the surface energies.

As evident from (Figure 2), the solid-phase nucleation exhibits an ordered dendritic crystal structure. The dendritic nucleus structure has been found to be surrounded by symmetrically distributed fine solid particles. As the reaction progresses, these particles are gradually depleted during nucleation which results into a dendritic crystal structure. There are two factors relating to conventional BZ reaction systems that might favor the formation of ordered dendritic crystal structure.[26,27] First, the dynamic instability (Mullins–Sekerka instabilities) generates a concentration gradient between nucleation centers and fine solid particles. The concentration gradient facilitates colloidal particles to fuse into the solid interfaces in a synchronized manner. The effective transport properties of the particles depend upon the diffusion coefficients that can allow particles to fuse either with higher or lower mobility. It has also been assumed that the dynamic instabilities could also dictate the orientated aggregation of fine solid particles during formation of dendritic nucleus structure. Second, surface anisotropy determines the randomness in the resulting structure. This can be induced by non-uniform surfaces of the metal catalysts and also due to probable multi crystal phases. In this circumstance, a diffusion mediated aggregation mechanism could facilitate coherent side branching in the dendritic crystal patterns.

In addition to this, a pair of metal catalysts (Fe^{2+}/Fe^{3+}; Ce^{3+}/Ce^{4+}) present in the reaction system participate in wave and pattern formation, during solution phase reaction. These metal ions remaine after reaction in inert form. Due to their non-uniform surfaces, they can provide long-lived dynamic heterogeneities to the reaction system.[28] This heterogeneity can build up a transportation gradient between nucleation sites and the symmetrically distributed colloidal particles. As expected, the fine solid particles are more than a single type which differs in diffusion coefficients. Depending upon characteristics and size of these particles, the diffusion coefficients allow aggregation with much higher or lower mobility toward the nucleation sites. Under diffusion conditions, this aggregation mechanism is similar to cycles of oscillations or periodic routes.[13,27] It results in fine tuned ordered structure of dendritic patterns, as observed during the experiment.

Growth of Tree/Bushes-Like Crystal Patterns. During colloidal-phase reaction, the dendritic nucleus center has been found to grow in specified geometry which results in tree/bush-like branched crystal patterns. The resulting morphology is shown in Figure 4, and a proposed graphical scheme, as shown in Figure 5a, demonstrates the apparent growth behavior and branching mode of tree/bush-like crystal patterns. By means of branching modes the morphology orders of tree/bush-like crystal patterns differ from spherulitic crystal patterns and seaweed-like crystal patterns are illustrated in Figures 5b and 5c respectively. The tree/bush-like crystal patterns exhibit a coherent side branching similar to the symmetric dendrites. It is observed that during growth, secondary and tertiary branching takes place successively which appears as densely branched morphology, whereas a spherulite composed fibrous network is oriented in radial direction which forms nearly spherical crystal morphology, which is clearly shown in Figure 5b. The seaweed-like crystal patterns (Figure 5c) exhibit broad growing tips that split intermittently and one of the newly formed branches and normally grow to predominate over the other.

The morphology of the studied tree/bush-like crystal patterns closely resemble some simulated DLA-like patterns.[15–19] Similar to the DLA model, the growth process begins from prerequisite nucleation sites. The solvent acts as a medium which allows the fine solid particles to aggregate toward nucleation site by random walks. The possible nucleus centers have been found to exhibit formation of akin crystal patterns. The possibility of fine solid particles to enter most exterior segments of the crystal surface are least, subsequently, the nucleation centers formed at later stage can start to grow at moderate rate while the growth rate of the nucleation centers formed in earlier stages become slow due to screening effect similar to the DLA experiment.[18]

Aggregation of colloidal particles takes part in growth of the tree/bush-like crystal patterns. These colloidal particles have been regarded as growth units which participated in the growth of tree/bush-like crystal patterns. The dimension of colloidal particles varies as characterized by SEM. This indicated that colloidal particles observed during reaction are not similar and may be obtained from diverse routes as described in the reaction mechanism. On the other hand, dissimilar crystal units control the randomization and synchronization which are essentially needed for growth of orderly crystal surfaces. Due to differences in diffusion coefficients, smaller particles may aggregate in the central or core region of the tree/bush structure, while much bigger particles toward exterior segments.

At micro scale, the tree/bush-like crystal patterns exhibit complex organizations. DLS study has been carried out for micro level descriptions of such complex and ordered structures. It has been suggested that the colloidal particles which participated in crystal growth are in nanometer scales ($d > 100$ nm). These particles have a well-built tendency to aggregate due to intermolecular interactions, whereas the stability of these aggregated structures is controlled by a balancing force between van der Waals attractions and Coulombic repulsions of colloidal particles. Additional enhancement in the van der Waals attraction and weakening the Coulombic repulsion force may increase the aggregation rates.[29–31] The intermolecular repulsive forces might be preventing colloidal particles to agglomerate. A viscous drag force by the reaction medium (solvent), acts to resist escaping particles from their aggregated structures. Although, the evaporation of solvents is expected during growth which can disturb the balance between aggregate particle and organized

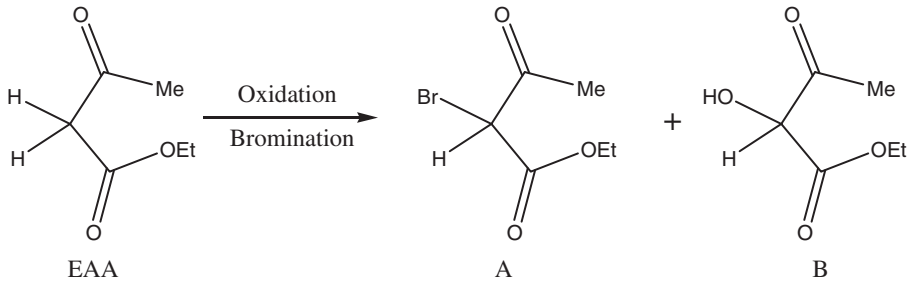

Scheme 1.

structures. But the process undergoes slow evaporation hence it facilitates crystal growth toward exterior segments. The growth of crystal surface is associated with decrease in the interfacial surface energy. Lowering the surface energy can provide an additional stability in the growing crystal structure.[26,27]

The driving force is an essential factor required for transportation of particles during growth. The emergence of the driving force can be described in two different ways: first, the process begins with phase separation which facilitates the change in physical state of the system. The difference in free energies of possible physical states generates a thermal gradient. Second, the dynamic instability due to Mullins–Sekerka is encountered during such phase separation. Dynamic instability can further destabilize the liquid–solid interface, resulting in emergence of a driving force which is also monitored by diffusion and surface energy. So it can be suggested that the emergence of the driving force arises due to the thermal gradient and dynamic instability of the reaction system.

As described, many sequential reaction processes are involved in the growth of tree/bush-like crystal patterns. To propose and describe an entire reaction mechanism is a complicated task. Nearly 24-reaction steps have been reported during solution-phase reaction (oscillatory reaction) of the BZ reaction. However, qualitative expressions of their reactions and growth mechanism of the tree/bush-like crystal pattern is proposed under two different schemes. Based on eq 2, two major products for the growth of tree/bush-like crystal patterns have been proposed in Scheme 1.

The products **A** and **B** could transform into some complexes with reacting metal ions. Fine solid particles, observed during colloidal phase, may be either individual products of **A** or **B** or their complexes. SEM study has been carried out which showed multiple product phase with different dimensions. It has been suggested that a probable derivative of SA along with product **A** or product **B** might take part in growth of tree/bush crystal patterns. A stable derivative of SA is shown in Scheme 2.

It has been reported that EAA can readily be brominated and hydrolyzed under controlled conditions. It can be considered that a derivative of EAA (often hydrolysis product) is associated with dual frequency (low- and high oscillatory phases) regimes. A short-lived oscillatory pattern observed during initial reaction might be bromination of hydrolyzed products of the EAA. The hydrolyzed products and brominated derivatives are unstable and can form complexes with Ce^{4+} or Fe^{2+}. The presence of metal ions, $Ce^{4+}$and iron Fe^{2+} have been confirmed from the EDS spectra as shown in Figure 6.

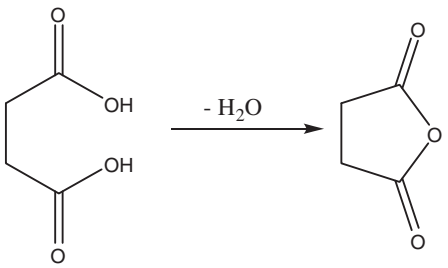

Scheme 2.

Similarly SA also undergoes oxidation/bromination during solution phase reactions. However, there are two active methylene (–CH_2–) groups and hence, reactivity toward oxidation/bromination is feeble compared to EAA. But, at high saturation where much solvent evaporates, H_2SO_4 (initially 0.42 M) becomes sufficiently concentrated. The remaining SA may dehydrate and transform into a stable 5-membered ring of succinic anhydride (SAA). Thus it has been suggested that SAA along with product **A** or product **B** or their complexes can control the growth of tree/bush crystal patterns. This explanation also emphasizes the multicrystal phases which facilitate randomization and synchronization of described crystal units during growth. To characterize the multicrystal phases and possible composition of the tree/bush crystal patterns, GC-MS analysis has been carried out. The results show (Figure 7) multiple peaks at retention times (min) of 11.58, 21.43, 23.36, and 36.44 with M^+ of 100, 146, 174, and 202 respectively. A prominent peak, at retention time (min) 11.58 was found to have (100%) ion abundance. The fragmentation patterns were searched in the Wiley registry and NIST mass library database. The fragmentation pattern with M^+ of 100 and 174 were found to be similar to SAA (NIST-192) and diethyl succinate (wiley-61781) respectively. Since SAA ions were found to be (100%) in the chromatogram, they can play an important role in the growth of tree/bush crystal patterns.

Morphological Transition in Crystal Patterns. The experiment has been carried out in the concentration range of organic substrates as [EAA] = 0.091–0.1325 mol dm^{-3} and [SA] = 0.110–0.1420 mol dm^{-3} respectively. It is evident from the study that dual substrates are essentially needed for growth of the crystal patterns. However, the crystal morphology has been found to change under varying concentrations of both substrates. One from each experimental condition with EAA and SA has been presented to illustrate the morphological transitions of crystal patterns, as shown in Figures 8a and 8b.

With increases in the concentration of EAA, densely branched patterns (DBP) have been obtained. DBP composed of long fiber-like crystal units which are found to be well-organized patterns and closely resemble fibrous spherulites of polymers. The result observed at concentration range ($[EAA] = 0.1225\,mol\,dm^{-3}$) is shown in Figure 8a. On the other hand, a symmetric branched pattern (SBP) composed of thick and expanded crystal units was observed on increasing the concentration of SA. Observations at concentration range ($[SA] = 0.1380\,mol\,dm^{-3}$) are shown in Figure 8b. The morphology of these crystal patterns was found to be similar to seaweed-like crystal patterns. It has been observed that both systems exhibit comparable nucleation and growth as suggested for tree/bush crystal patterns. One difference between DBP and SBP is the branching mode during crystal growth. The branching modes and the characteristic morphology of spherulitic crystal patterns and seaweed-like crystal patterns can also be observed in the proposed graphical scheme which is shown in Figures 5b and 5c respectively. However, the transitions in morphology of crystal patterns can be explained in two different ways. First, when SAA is readily formed (SA-rich system in Scheme 2), these molecules are effectively involved in crystal growth. Due to the crystallizing nature of SAA, thick and expanded crystals are copiously formed which results in SBP crystal morphology. Second, the transition in crystal morphology has been explained on the basis of thermodynamic distances from the equilibrium positions.[14,32,33] This consideration has been associated with extent of the reaction and solvent evaporation rates which were effective in the EAA-rich system. The BZ-like systems may retain their excitability even for a longer period, which could keeps the reaction far from equilibrium. The high solvent evaporation has been found in EAA-rich systems, which might generate much higher driving forces within the reaction system. The growth fronts of crystal surfaces become destabilized due to high driving force and by contribution of mass or heat diffusion. This further increases the surface instability which leads to the formation of DBP with fibrillar organizations.

Morphological Study of Tree/Bush Crystal Patterns. The branching orders of tree/bush crystal patterns were considerably characterized with the help of OPM. The crystal pattern was composed of large numbers of well-aligned crystals as branches. The branches associated with a common point (nucleus center), correspond to the primary branches which form the initial outline of the tree/bush crystal patterns. Secondary and tertiary branches are in turn associated with primary branches which ultimately results in densely branched crystal patterns. Due to diffusion field restrictions, all three kinds of branches, as observed, do not intersect with each other. It implies that the aggregation process has not been completely random.

More than two types of crystals are involved in the growth of tree/bush patterns as observed in SEM microphotographs (Figure 9). The array of long crystals seen in the background may have resulted from a component of SA or its derivatives. We assume that these crystals can play a major role in the formation of main architecture of tree/bush patterns. Some porous types of crystals can also be seen in microphotographs. These porous crystals have different geometries which display joint and socket-like fabrications as observed in SEM microphotographs. Based on crystal geometries and unique fabrications, the possible products (as proposed in Schemes 1 and 2) might be self-organized, before/during crystal growth.

X-ray Analysis. The X-ray powder diffraction spectrum of the tree/bush patterns, as shown in Figure 10B, has a number of sharp peaks with high intensity as a result of highly crystalline phase. Consequently, some broadened peaks, (beyond 50°) having low intensities are observed in the spectrum which attributes to a certain amorphous phase, that not only serves as a binding of multi crystal phases but also plays an important role in molding the tree/bush patterns. In the resulting powder X-ray spectrum of pure SA, shown in Figure 10A, fewer peaks appear between 33 to 50° which is in contrast with tree/bush-like pattern materials. However few peaks in highly crystalline material and pure SA were found at similar positions, having different intensities. Thus it is suggested that the tree/bush-like crystal patterns have not resulted from simple aggregation of SA or its derivative but due to involvement of multi crystal phases. The average crystal size of SA and tree/bush crystals has been estimated as 46.76 and 78.34 nm respectively, using the Scherrer formula.[34]

Characterization Using FTIR. The FTIR spectrum of the tree/bush crystal materials is shown in Figure 11. The absence of a broad peak in the spectrum ranging between 2500–3000 cm^{-1} is due to the absence of carboxylic acid groups. The peaks at 1697, 1514, and 1415 cm^{-1} are the characteristic peaks of carbonyl (CO) groups. The consecutive peaks in this region further assert that the carbonyl groups are associated with cyclic structure or possibility of the coordinate linkage. The peaks at 1056 and 1008 cm^{-1} depict anhydride groups. Peaks at 3055 cm^{-1} are due to C–H stretching related to highly ordered structure of the hydrocarbon. One peak at 3741 cm^{-1} is either for hydrogen bonding or water in coordinated state. The possibility of Metal–Oxygen (M–O) bonds and their corresponding peaks can also be observed in the spectrum between the ranges of 500–600 cm^{-1}.

Conclusion

The growth of tree/bush-like crystal patterns in a dual organic substrate (EAA/SA) of a BZ reaction system is reported. The morphology of the tree/bush-like patterns resembles simulations of DLA patterns. The colloidal particles have been formed during reaction which plays a significant role for solid-phase nucleation initially and subsequently in the growth of tree/bush-like crystal patterns. The expressions of possible reactions has been shown and properly described. With the help of the fundamentals of DLA mechanism, the growth behavior and the fractal characteristics of the tree/bush-like crystal patterns are described. The excitable condition of the BZ reaction solution and fluctuation in driving force were two factors which kept the reaction system far from equilibrium. This reasonably contributed to transition in morphology of the tree/bush-like crystal patterns.

Authors acknowledge to the University Grant Commission (UGC) for financial support. Authors would like to take an opportunity to thank Dr. A. K. Chatterjee, Prof. and Head, Department of Space Engineering and Rocketry, Dr. (Mrs)

Usha Jha, Prof. and Head, Department of Applied Chemistry, BIT, Mesra, Ranchi for their infrastructural and moral support and also valuable inputs for improvement of the manuscript contents. Authors are grateful to Dr. Prasana Kumar David, Associate Professor and Head, Department of English, Gossner College, Ranchi University, Ranchi and Abur Jasser Aulla, Assistant Professor, Computer Science and Engineering, BIT, Mesra for their valuable inputs for improvement of the manuscript content.

References

1 I. R. Epstein, J. A. Pojman, *An Introduction to Nonlinear Chemical Dynamics: Oscillations, Waves, Patterns, and Chaos*, Oxford University Press, New York, **1998**.

2 I. R. Epstein, K. Showalter, *J. Phys. Chem.* **1996**, *100*, 13132.

3 R. P. Rastogi, M. M. Husain, P. Chand, G. P. Misra, M. Das, *Chem. Phys. Lett.* **2002**, *353*, 40.

4 I. R. Epstein, J. A. Pojman, *Chaos* **1999**, *9*, 255.

5 T. Yamaguchi, I. R. Epstein, M. Shimomura, T. Kunitake, *Chaos* **2005**, *15*, 047501.

6 I. R. Epstein, J. A. Pojman, O. Steinbock, *Chaos* **2006**, *16*, 037101.

7 K. Iwamoto, S. Mitomo, J. Fukide, T. Shigemoto, M. Senō, *Bull. Chem. Soc. Jpn.* **1982**, *55*, 709.

8 A. Toramaru, T. Harada, T. Okamura, *Physica D* **2003**, *183*, 133.

9 R. Yoshida, *Bull. Chem. Soc. Jpn.* **2008**, *81*, 676.

10 T. Kyu, H.-W. Chiu, A. J. Guenthner, Y. Okabe, H. Saito, T. Inoue, *Phys. Rev. Lett.* **1999**, *83*, 2749.

11 L. Wu, Y. Wu, Y. Lü, *Mater. Res. Bull.* **2006**, *41*, 128.

12 X. Zhai, W. Wang, G. Zhang, B. He, *Macromolecules* **2006**, *39*, 324.

13 K. Fukami, S. Nakanishi, H. Yamasaki, T. Tada, K. Sonoda, N. Kamikawa, N. Tsuji, H. Sakaguchi, Y. Nakato, *J. Phys. Chem. C* **2007**, *111*, 1150.

14 J. Li, Y. Shi, Q. Cai, Q. Sun, H. Li, X. Chen, X. Wang, Y. Yan, *Cryst. Growth Des.* **2008**, *8*, 2652.

15 R.-F. Xiao, J. I. D. Alexander, F. Rosenberger, *J. Cryst. Growth* **1990**, *100*, 313.

16 T. A. Witten, L. M. Sander, *Phys. Rev. Lett.* **1981**, *47*, 1400.

17 L. M. Sander, *Nature* **1986**, *322*, 789.

18 J. S. Langer, *Rev. Mod. Phys.* **1980**, *52*, 1.

19 P. Meakin, F. Family, T. Vicsek, *J. Colloid Interface Sci.* **1987**, *117*, 394.

20 S. C. Ferreira, *Eur. Phys. J. B* **2004**, *42*, 263.

21 L. F. Salter, J. G. Sheppard, *Int. J. Chem. Kinet.* **1982**, *14*, 815.

22 R. M. Noyes, *J. Phys. Chem.* **1990**, *94*, 4404.

23 P. Ruoff, *J. Phys. Chem.* **1984**, *88*, 1058.

24 C. Peralta, C. Frank, A. Zaharakis, C. Cammalleri, M. Testa, S. Chaterpaul, C. Hilaire, D. Lang, D. Ravinovitch, S. G. Sobel, H. M. Hastings, *J. Phys. Chem. A* **2006**, *110*, 12145.

25 Z. Nagy-Ungvarai, S. C. Muller, J. J. Tyson, B. Hess, *J. Phys. Chem.* **1989**, *93*, 2760.

26 L. Gránásy, T. Pusztai, T. Börzsönyi, G. I. Tóth, G. Tegze, J. A. Warren, J. F. Douglas, *Philos. Mag.* **2006**, *86*, 3757.

27 V. Ferreiro, J. F. Douglas, J. Warren, A. Karim, *Phys. Rev. E* **2002**, *65*, 051606.

28 A. Gómez, J. J. Luque, A. Córdoba, *Chaos, Solitons Fractals* **2005**, *24*, 151.

29 I. Lee, J. S. Ahn, T. R. Hendricks, M. F. Rubner, P. T. Hammond, *Langmuir* **2004**, *20*, 2478.

30 Y. Cheng, Y. Wang, D. Chen, F. Bao, *J. Phys. Chem. B* **2005**, *109*, 794.

31 T. Hashimoto, *Bull. Chem. Soc. Jpn.* **2005**, *78*, 1.

32 A. G. Marangoni, M. Ollivon, *Chem. Phys. Lett.* **2007**, *442*, 360.

33 H. You, J. Fang, F. Chen, M. Shi, X. Song, B. Ding, *J. Phys. Chem. C* **2008**, *112*, 16301.

34 Y. S. Shi, *Phys. Lett. A* **2003**, *319*, 555.